Journal of Mechanical Research and Application, JMRA
ISSN: 2251-7383, eISSN:2251-7391
Vol. 3, No. 1, 2011, 37-47

Investigation of the Flow and Cavitation in a Butterfly Valve

Hossein Nazary[1*], Nafise Aalipour[2], Mansour Alizadeh[3]

Received: 17 May 2011; Accepted: 2 Jan. 2012

Abstract: Since knowledge on hydrodynamic torque of a butterfly valve is very important for butterfly valve design, its hydrodynamic torque is investigated in this paper. In reality, the investigation of the loss coefficient and torque from some experiments will take a long time and a lot of money. This paper presents a statistical study of the flow past the butterfly valve in a static analysis using commercial fluid dynamics software fluent. The simulation was done for 16 different positions of the valve disk including 0°, 5°,10°, 15°, 20°, 30°, 35°, 45°, 50°, 55°, 65°, 70°, 75° and 80°. The value of pressure in the pressure inlet was set to be 16 bars. The study focuses on the investigation of the characteristics of loss coefficient, torque behavior and flow field of the 262 mm butterfly valve. The results show that the loss coefficient is directly dependent on the position of the valve disk and by increasing the angle of the valve disk the value of loss coefficient increases and the value of torque increases until about 10°-20° and then decreases. By comparing between the experimental and statistical data, acceptable relationships were observed.

Keywords: Butterfly Valve, Hydrodynamic Torque, Loss Coefficient, Dimensionless Torque Coefficient

1. Introduction

The opened-closed controller or safety unit for fluid-flow in piping system is an important element in every piping configuration. One of the most well-known is butterfly valve. The butterfly valve has 3 main components consisting of the body, the shaft and the valve disk. It is commonly set up into the system to induce the flow as well as acting as a safety device. Not only its low cost but also its simple mechanical assembly that makes the butterfly valve to be useful over any other valves. Butterfly valve also provides the large flow capacity at a completely open position. Moreover when compared to various valve designs of a comparable size, butterfly valve are also advantageous.

The main standard variables of butterfly valve, are classified as: the loss coefficient and the hydrodynamic torque. The torque acting on closing valve may be resolved into several components [1]. This may be written as (Eq. 1):

$$T_t = T_b + T_{cg} + T_d + T_p + T_h \quad (1)$$

Where T_b is bearing torque, T_{cg} is torque imposed by an offset center of gravity of the valve, T_d is hydrodynamic torque, T_p is the torque due to packing torque and T_h is torque due to the hydrostatic pressure. The sign convention used in this study is for torque to be positive when acting in the closing direction. Components T_b and T_p always act in the opposite direction to the valve closing direction. Components T_d and T_{cg} will depend on the valve geometry, and may act in either direction [1,2].

It is common to express the hydrodynamic torque T_d in the form of a dimensionless torque coefficient. The two most common definitions are:

$$C_{t1} = \frac{T_d}{\left(\frac{1}{2}\ p\bar{u}^2\right)D^3} \quad (2)$$

$$C_{t2} = \frac{T_d}{(\Delta P)D^3} \quad (3)$$

Where ΔP represents the static pressure different-

1*. Corresponding Author: M. Sc. Student, Mechanical Engineering Department, Science and Technology University, Tehran, Iran (Hossein_Nazary@mecheng.iust.ac.ir)
2. M. Sc. Student, Mechanical Engineering Department, Science and Technology University, Tehran, Iran (aalipourn@mecheng.iust.ac.ir))
3. Associate Professor, Mechanical Engineering Department, Science and Technology University, Tehran, Iran (ma_alizadeh@iust.ac.ir)

ialacross the valve. For model testing, the downstream pressure should be measured at least 10D downstream to allow for sufficient pressure recovery and the upstream pressure should be measured at least 2D upstream [1].

Solliec and Danborn [3] compared torque coefficient results presented as Eqs. (2) and (3) to be less sensitive to the effects of other system losses such as bends and elbows and thus more useful definition for comparing valve torque characteristics in different valves. Eq. (3), however, is the more commonly used for a 'classic' approach. The dynamic pressure reduces as the valve is closed, which can give very high values of C_{t1} at high valve angles $(a > 65^0)$. However, maximum hydro-dynamic torque occurs at much lower angles and is better reflected by Eq. (3) as the static pressure does not vary significantly.

Head loss is a measure of the reduction in the total head of the fluid as it moves through a fluid system. It can be explained as the energy equation for a steady incompressible flow:

$$\frac{p_1}{g} + b_1 \frac{u_1^2}{2g} + z_1 = \frac{P_2}{g} + b_2 \frac{u_2^2}{2g} + z_2 + h_l \qquad (4)$$

Head loss is unavoidable in real fluids. It is presented because of the friction between the fluid and the walls of the pipe and the friction between adjacent fluid particles as they move relatively one to another. Frictional loss is that part of the total head loss that occurs as the fluid flows through straight pipes. However, most pipe systems consist of more straight pipes. The other components such as bends, valves, gates, etc. installed into the system add head losses to the overall head loss.

The head loss associated with flow through a valve is commonly known as a minor loss. The most common method is to specify the loss coefficient, K_L which is defined as:

$$K_L = \frac{h_L}{u^2 / 2g} = \frac{\Delta P}{\frac{1}{2} p u^2} \qquad (5)$$

It can be shown as:

$$\Delta P = K_L \frac{1}{2} p u^2 \quad \text{or} \quad h_L = K_L \frac{u^2}{2g} \qquad (6)$$

2. Scope of investigation

The Reynolds number rang used in this study shows in Table 1. A schematic diagram of the valve geometry is shown in Fig. 1. The valve is symmetrical about the Y-Z plane and maintains a uniform maximum leaf-section thickness t of 6 mm along its axis. Actually, the economic reason becomes an important factor of research and development. The symmetric model as shown in Fig. 1 was created below under this factor. The size of domain is therefore decreased thus increasing the speed of the statistical simulation.

The boundary conditions, used in this study was set to be as in Table 2. In order to get enough entry length and to avoid a non-fully developed flow, an upstream and a down-stream length were set to be several times the pipe diameter.

3. Numerical model

Nowadays numerical method becomes powerful technique and commonly utilized to solve a wide variety of flow problems. The differential equations that govern a flow of Newtonian fluids based on the Navier-Stokes equation. It can be compactly expressed in vector notation as:

$$r\left[\frac{\partial u}{\partial t} + u.\nabla u\right] = -\nabla P + rg + m\nabla^2 u \qquad (7)$$

Along with the continuity equation:

$$\nabla . u = 0 \qquad (8)$$

The standard $k - \varepsilon$ model is a semi-empirical model based on model transport equations for the turbulence kinetic energy (k) and its dissipation rate (ε). The turbulence kinetic energy, k and its rate of dissipation, ε are obtained from the following transport equations:

$$\frac{\partial (rk)}{\partial t} + \frac{\partial (rku_i)}{\partial x_i} = \frac{\partial \left[\left(m + \frac{m_t}{s_k}\right)\frac{\partial k}{\partial x_j}\right]}{\partial x_j} + G_k + G_b - re - Y_m + S_k \qquad (9)$$

$$\frac{\partial (re)}{\partial t} + \frac{\partial (reu_i)}{\partial x_i} = \frac{\partial \left[\left(m + \frac{m_t}{s_e}\right)\frac{\partial e}{\partial x_j}\right]}{\partial x_j} + C_{1e}\frac{e}{k}(G_k + C_{3e}G_b) - C_{2e}\frac{re^2}{K} + S_e \qquad (10)$$

Table 1. the Reynolds number range used in this study

angle	Reynolds Number
0	14916356.7
5	15483045.9
10	15613319.7
15	13831824.9
20	12646333
25	11216577.6
30	9982233
35	8624128.2
45	6126127.3
50	5123018.7
55	4292523
60	3751886.6
65	3289414.4
70	2960473
75	2712952.7
80	2550110.4

Table 2. The boundary condition of each domain

Surface domains	Boundary conditions
inlet	pressure inlet
outlet	Pressure outlet
symmetry	symmetry
Valve disk	wall
Pipe surface	wall

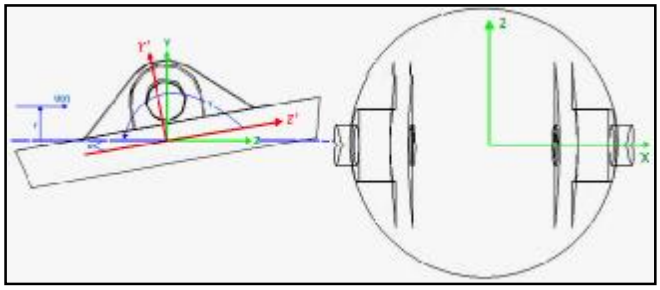

Fig. 1. Butterfly valve arrangement.

In these equations, G_k represents the generation of turbulence kinetic energy due to the mean velocity gradients. G_b is the generation of turbulence kinetic energy due to buoyancy. The quantity Y_m represents the contribution of the fluctuating dilation incompressible turbulence due to the overall dissipation rate. C_{1e}, C_{2e} and C_{3e} are the constant. s_k and s_e are the turbulent Prantel number for k and e, respectively S_K and S_e are user defined source terms [4].

The turbulent viscosity m_t is computed by combining k and e as follows:

$$m_t = r\, C_m \frac{k^2}{e} \tag{11}$$

Where C_m is a constant. The model constants C_{1e}, C_{2e}, C_m, s_k and s_e have the following default values:

$$C_{1e} = 1.44, C_{2e} = 1.92, C_m = 0.09, s_k = 1, s_e = 1.3$$

These default values have been determined from the experiments with air and water for fundamental turbulent shear flows including homogeneous shear flows and decaying isotropic grid turbulence. They have been found to work fairly well for a wide range of wall-bounded and free shear flows. The valve geometry was created using CATIA software and imported into ANSYS design Modeller.

A rubber seal about the rim of the valve was not included in the model to avoid problems associated with meshing very small sliver volumes. The gap closed by the seal is small and was not expected to have a significant influence on the flow through the valve. The flow was assumed to be symmetrical about the valve Z-Y centreplane, and thus only half of the flow field was modelled by applying a symmetry boundary condition. Further details of the geometry creation are given in Haynes [5].

The computational domain was divided into three main sections: upstream, near valve section, and the downstream. Upstream and downstream sections were meshed using an inflated layer of hexahedral elements on the walls, with triangular-based prism elements in the center. A layer of inflated elements used on the valve face to improve modeling of the boundary layer. The surrounding mesh consisted of tetrahedral elements. Meshes were generated for valve angles between 0^0 and 80^0 in steps of 5^0. The total number of element contained in each mesh varied between 800000 and 1000000. Fig. 2 shows the mesh on the valve symmetry plane at a valve angle of $a = 60^0$.

The near wall flow was modeled using ‘‘automatic’’ wall functions, which automatically switch between a low Reynolds number approach to scalable wall functions depending on local conditions and the wall normal element spacing [6]. This effectively removes the lower limit of y^+ required by standard wall functions. The y^+ values of the mesh varied with both inlet Reynolds number and valve angle, but were mostly less than 200, which is within the specifications given in the software documentation [6]. Solution times were generally around 20-25 hours using Aacpi/genuineinte l5.1.2600.0 system.

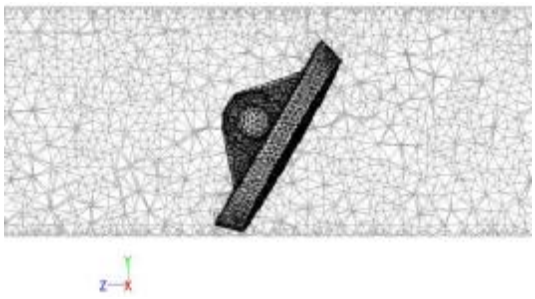

Fig. 2. CFD mesh on the X-Y symmetry plane for a valve angle of a = 60°

4. Comparison between different turbulence models

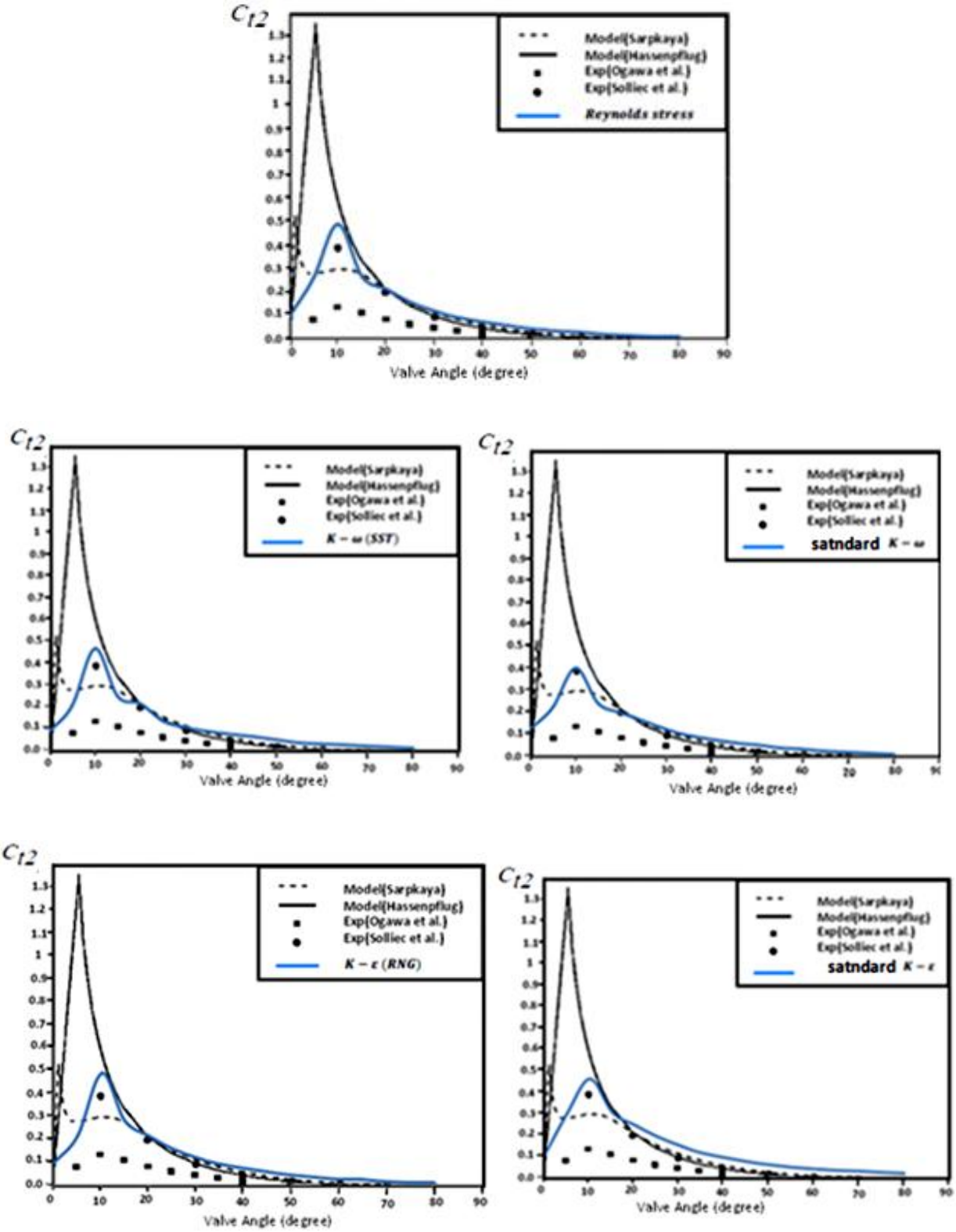

Fig. 3. Experimental and theoretical and CFD torque coefficient (C_{t2}).

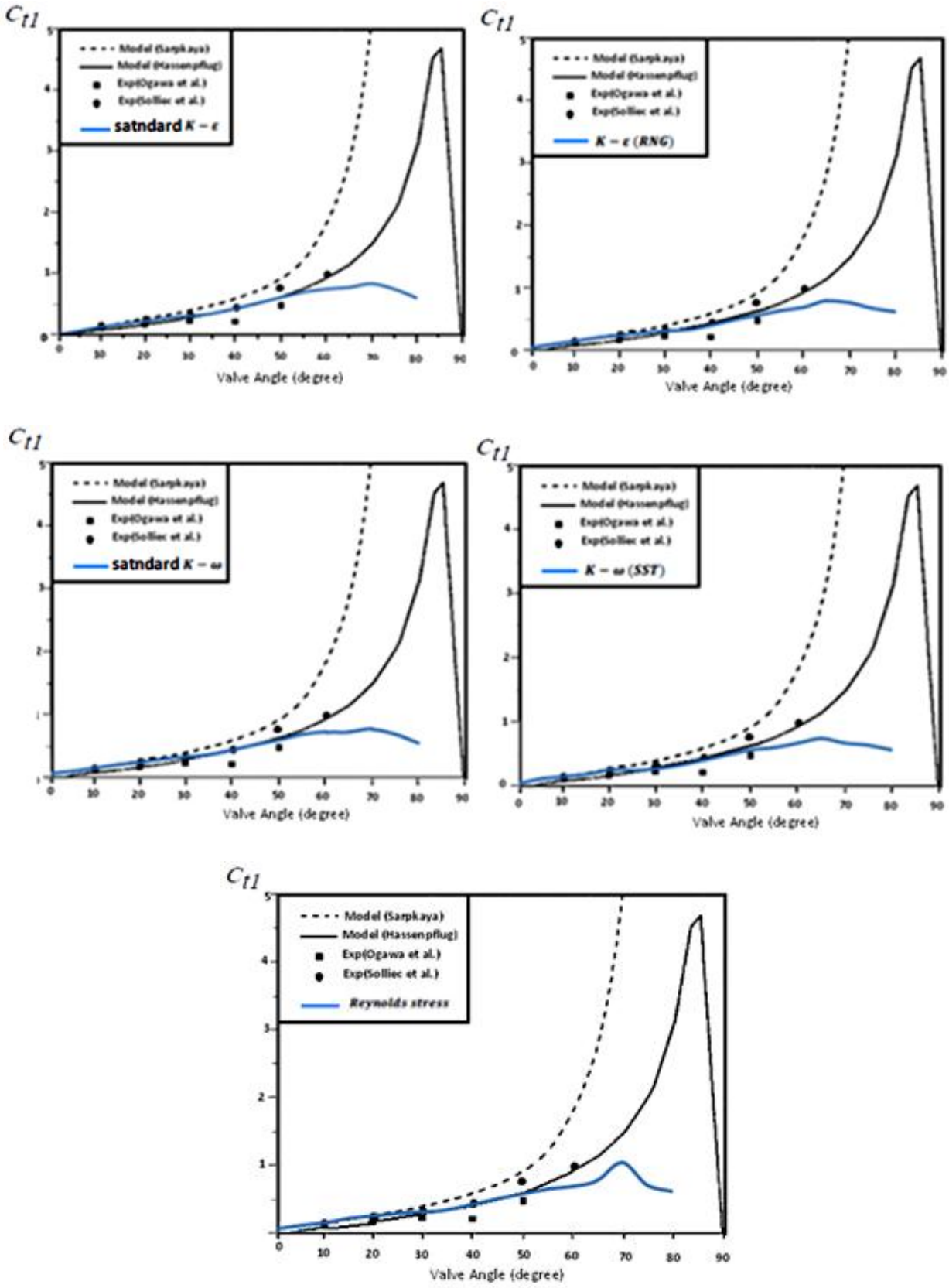

Fig. 4. Experimental and theoretical and CFD torque coefficient (C_{t1}).

5. Inlet velocity profile

The upstream velocity profile was compared against the standard 'power law' to verify that the flow had developed by the time it reached the valve. The power law may be expressed as:

$$\frac{U}{U_{max}} = (1-\frac{r}{R})^{\frac{1}{n}} \qquad (12)$$

Where the index n was determined by applying a curve fit to the predicted velocity profile. These were determined as 100 for our case. Schilichting [7] used this approach to determine the indices for smooth pipe flow data at lower Reynolds numbers than those considered in this study.

Fig. 5 compares the predicted velocity profile from CFD and power law at a location D axially upstream from the valve shaft axis for $a = 0^0$. Reasonable agreement is observed in the near wall region and in the center region but sometimes it deteriorates slightly toward the center. It is possible that the flow has not fully developed although Schlichting [7] shows that the power law becomes increasingly inaccurate towards the center of the flow $(\frac{r}{R} < 0.2)$ and produces an unrealistic velocity gradient at the center.

6. Mesh resolution

A mesh refinement study was achieved for the valve that is shown in Fig. 6. The mesh was coarsened equally in all directions for each subsequent trial. The number of elements in the inflated wall layer was changed to maintain an acceptable aspect ratio.

However the first element height and expansion ratio of the inflated wall layers were not changed to avoid altering boundary layer modeling. These results suggest that sufficient resolution was provided by the mesh of around 800000 elements used for the purposes of this study.

7. Description of flow field

A sequence of plots showing the mid-valve flow field no the X-Y symmetry plane is shown in Fig. 7. At $a = 10^0$, no separation observed at mid-plane. Although not shown a small region of separated flow forms behind the valve close to the wall.

For $a = 20^0$ a small separation forms at mid-plane but the flow appears to reattach. The extent of this separation increases with valve angle, so that most of the downstream valve surface is separated at $a = 45^0$. Further increasing the valve angle increases the extent of the downstream flow separation. Despite this, the downstream length of flow domain was sufficiently long to prevent reverse flow at the outlet.

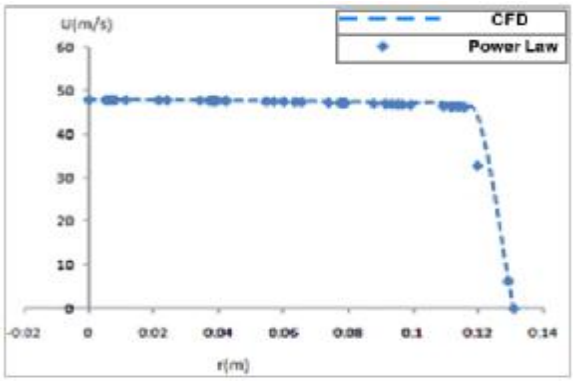

Fig. 5. Velocity distribution 2D upstream from the valve axis a =0°.

A dominant feature of the downstream flow is a counter-rotating streamwise vortex pair that develops at all non-zero valve angles. Since the valve is at an angle to the upstream flow, the pressure differential across the valve directs fluid downward near the sides, creating a

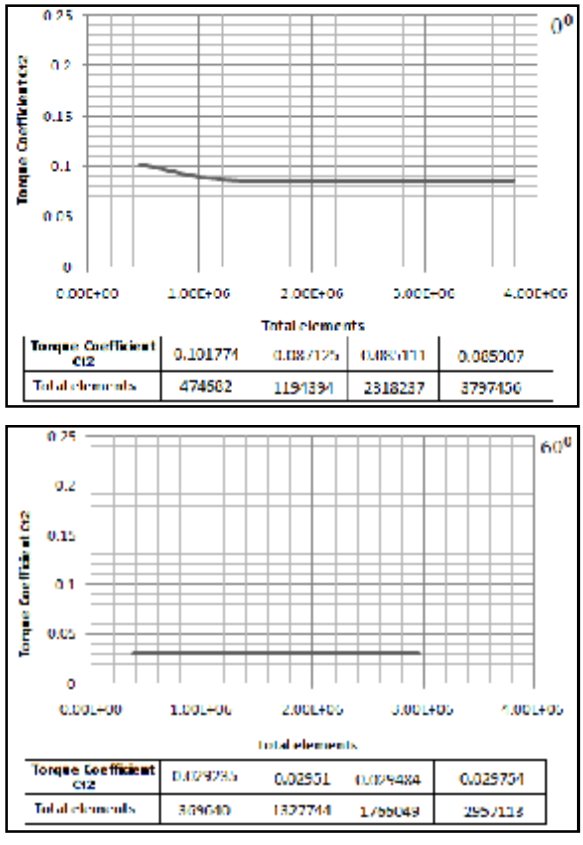

Fig. 6. Mesh resolution test.

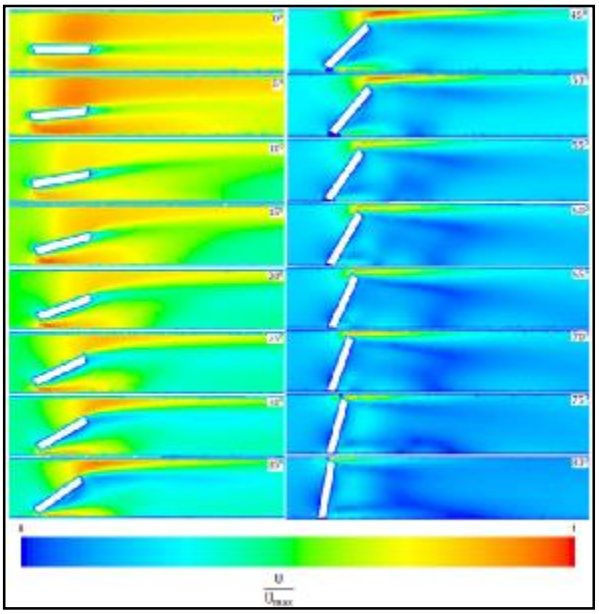

Fig. 7. Valve flow field on X-Y symmetry plane.

swirling flow. The strong vortical flow persists throughout the whole downstream flow domain. This also implies the existence of a lift force perpendicular to the pipe axis. Visualizations of this secondary flow are shown in Figs. 8 and 9.

8. Results and discussion

Figs. 10 and 11 compare the two different dimensionless torque coefficients of the butterfly valve calculated by statisticalmodel with experimental data and with Hassenpflug and Sarpkaya's models [8]. The curves qualitatively agree in terms of shape and sign, with maximum torque coefficient occurring near a =10°. However the maximum torque from the experimental results is significantly less than predicted. This difference may partially be explained by cavitation which will alter the flow pattern around the valve and consequently the torque required to close the valve. The CFD results may have been influenced by the use of symmetry boundary condition. For example, use of symmetry plane in the flow about a cylinder will interrupt eddy shedding.

Figs. 10 and 12 show that hydrodynamic torque is better reflected by C_{t2} and maximum of them occurs at a =10°-15°. Fig. 13 shows the value of loss coefficient from 0° to 90° position of 262 mm valve disk in static analysis. It was found that the k value is proportional to the disk position. By increasing the angle of the disk, the k value becomes greater until it reaches 51.25 at 80°.

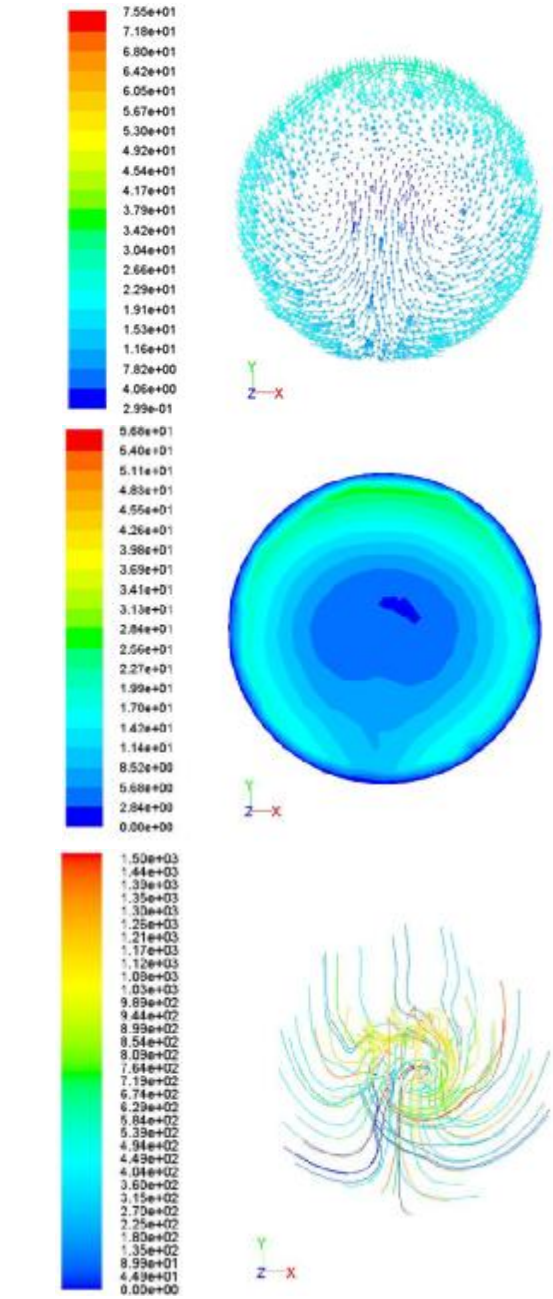

Fig. 8. Velocity vectors, contours and pathline on axial plane 2D downstream from the valve axis at a =60°.

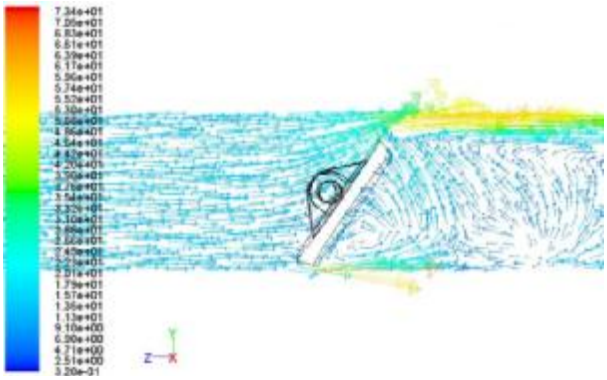

Fig. 9. Instantaneous velocity vectors shpwn on a Y-Z plane at a =55°.

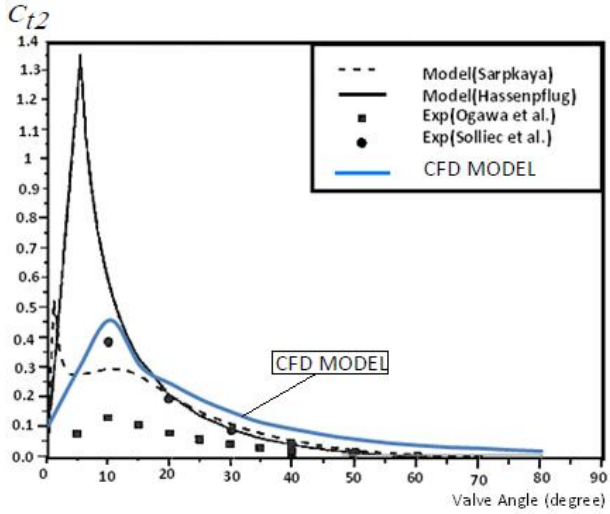

Fig. 10. Experimental and theoretical and CFD torque coefficient (C_{t2}).

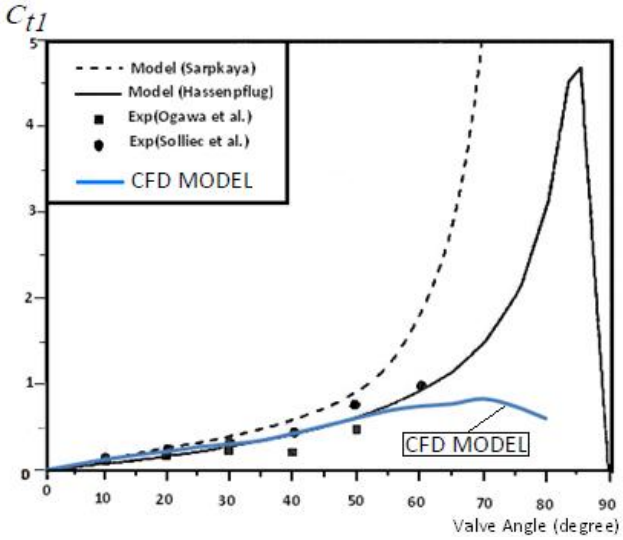

Fig. 11. Experimental and theoretical and CFD torque coefficient (C_{t1}).

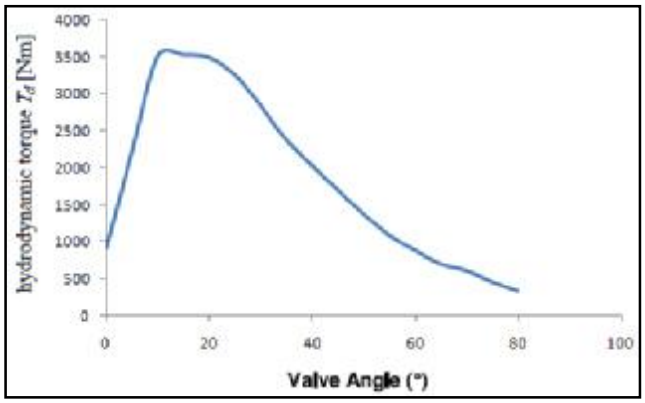

Fig. 12. The characteristic of the hydrodynamic torque.

It is also found that the flow around the valve, in position 75°, showed high turbulent condition behind the butterfly valve due to the smaller section area of the flow.

Researches show that size scale effects influence only incipient and critical levels of cavitation. The resulting equations recommended for making **s**ize **s**cale effect**s** adjust**s**ments (SSE) on incipient and critical are:

$$s = SSE(s_{ref} - 1) + 1 \tag{13}$$

$$SSE = \left(\frac{D}{d}\right)^{Y} \tag{14}$$

$$Y = 0.3K^{-0.25} \tag{15}$$

In which K is the valve loss coefficient s_{ref} is reference cavitation data for a valve of size d and s is the cavitation index value scaled to a valve of size D; which can be larger or smaller than the reference valve of size d. These equations are valid for orifices and valves.

When experimental data for sigma at incipient, critical or incipient damage are plotted on a log-log scale versus $P_1 - P_V$, the result is a series of straight lines with approximately constant slope. There is one line for each valve opening. The data produce simple scale effects equations which are valid for incipient, critical and incipient damage. The resulting equations are:

$$s = PSE(s_{ref} - 1) + 1 \tag{16}$$

$$PSE = \left(\frac{P_1 - P_V}{P_{1ref} - P_{Vref}}\right)^{X} \tag{17}$$

In which s_{ref} is experimentally determined reference cavitation index value evaluated at an absolute reference test pressure P_{1ref} and reference absolute vapor pressure P_{Vref}. The exponent X has been evaluated from extensive experimental data. P_1 and P_V are the absolute pressures at which the adjusted sigma is desired. When there are no pressure scale effects $X = 0$.

Figs. 13-16 show experimental and statisticaldata identifying the flow coefficient, discharge coefficient, loss coefficient, cavitation coefficient and the six cavitation limits for a 262 mm butterfly valve. Note that

the cavitation data are correlated using C_d rather than valve opening. Using C_d is the recommended basis of comparison for different valves because it bases the comparison on the energy dissipating capability of the valve, not just on percent valve opening. The upper plots allow the user to relate the C_d values in the sigma plot to valve opening and to C_V. The difference between statistical and experimental results is because of the different disks used in statistical and experimental studies. They also allow the reader to compare the data with similar data for other butterfly valves to see how similar they are. If the valve under consideration has similar C_V and/or C_d curves, the cavitation data in Fig. 16 should apply to the other valve.

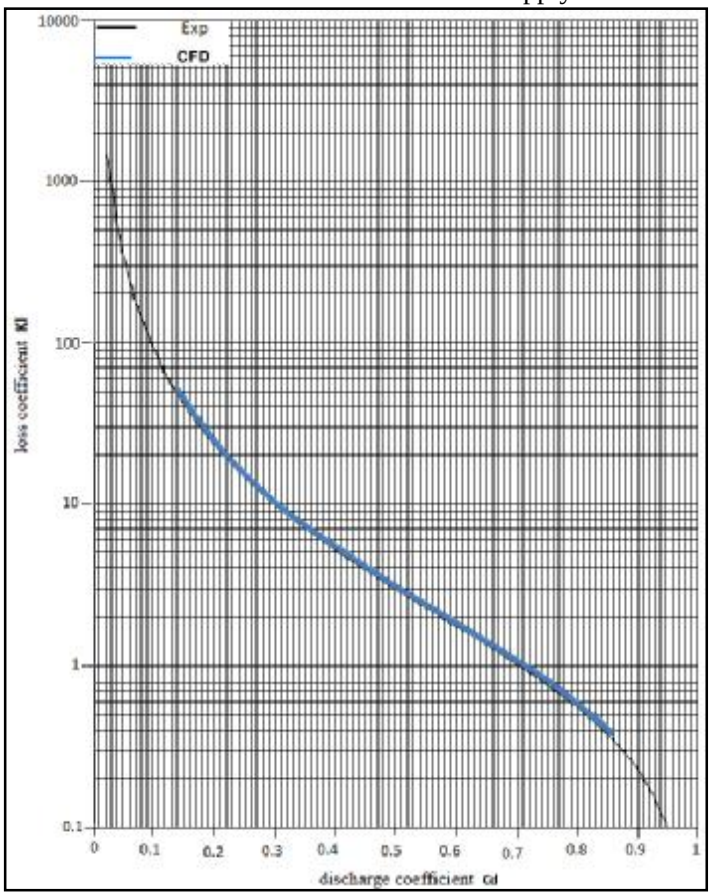

Fig. 13. The characteristic of the loss coefficient.

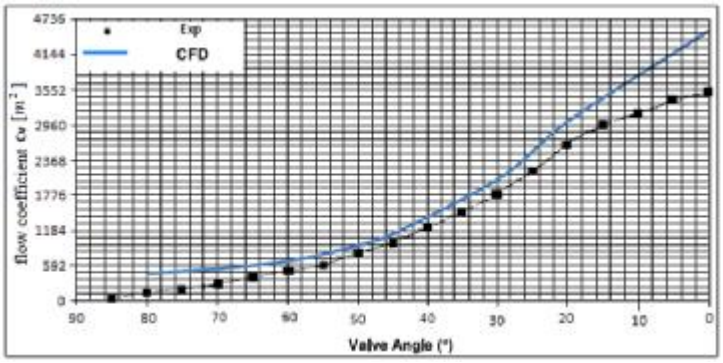

Fig. 14. The characteristic of the flow coefficient.

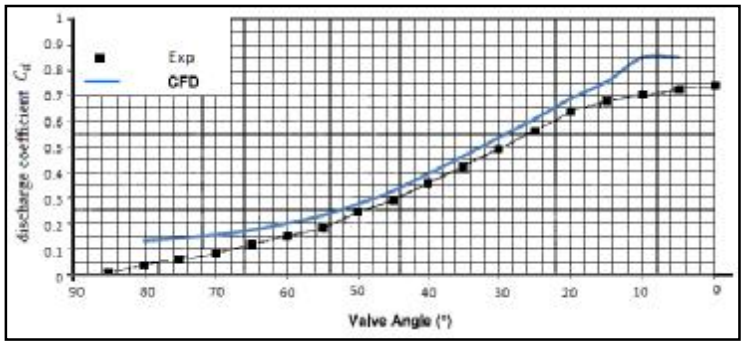

Fig. 15. The characteristic of the discharge coefficient.

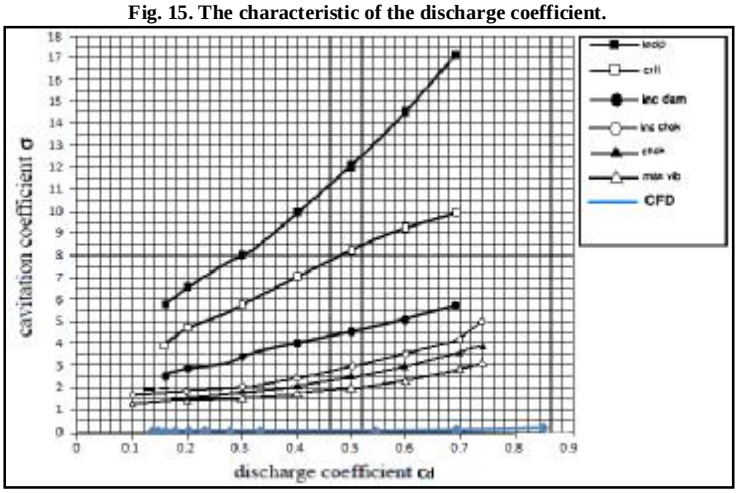

Fig. 16. The characteristic of the cavitation coefficient.

8. Conclusions

The investigation of the flow through a butterfly valve was done by statistical method to reach the characteristic of loss coefficient and torque behavior. The statistical simulation was done in static analysis under the butterfly valve size of 262 mm diameter at the position of 0°, 5°,10°, 15°, 20°, 30°, 35°, 45°, 50°, 55°, 65°, 70°, 75° and 80° of the valve. It was found that for $a > 20^0$ the extent of separation increases with an angle so that most of the downstream valve surface is separated at a = 45°. A counter-rotating stream wise vortex pair that develops at all non-zero valve angles is a dominant feature of the downstream flow.

From this investigation, it was found that the maximum value of the torque appears around $10^0 - 20^0$ position of the butterfly valve. The hydrodynamic torque T_d was expressed in the form of two dimensionless torque coefficients and when the comparison between the experimental and statistical results was made it was found that they are acceptable. Statistical results showed that the loss coefficient is directly dependent on the position of the valve and by increasing the angle of the valve disk the value of loss coefficient increases. Finally the statistical results can be improved in the future. By changing the turbulent model, the statistical results will be more accurate. To have a better description of the physics of the flow past the butterfly valve, the RNG $K-e$ model can be used. The Reynolds stress model (RSM), which can give the most accurate results is another interested model even if it will take a long time for calculation.

Nomenclature

C_{t1}	torque coefficient defin $1 = T_d / (\frac{1}{2} r\bar{u}^2) D^3$
C_{t2}	torque coefficient defin $2 = T_d / (\Delta P) D^3$
K_L	loss coefficient defin $= 2gh_L / u^2$
h_L	head loss defin $K_L u^2 / 2g$ $[m]$
g	specific weight $[kg / m^2 s^2]$
Z	elevation head $[m]$
P	Pressure $[Pa]$
T	Torque $[Nm]$

T_b bearing torque $[Nm]$

T_{cg} torque due to offset center of gravity $[Nm]$

T_d hydrodynamic torque $[Nm]$

T_h hydrostatic torque $[Nm]$

T_p packing torque $[Nm]$

u velocity $[m/s]$

$\bar{u}$ mean velocity $= Q/p\ R^2 [m/s]$

u_{max} local maximum velocity $[m/s]$

a valve angle relative to close position $[\mathbf{o}]$

r density of water $[kg/m^3]$

m dynamic viscosity of water $[Pa.s]$

m_t dynamic turbulent viscosity of water defin $= r\ C_m K^2 / e [Pa.s]$

K turbulence kinetic energy $[m^2/s^2]$

e turbulence dissipation rate $[m^2/s^2]$

D diameter of valve and housing $= 2R[m]$

R radial distance from centerline $[m]$

G_K the generation of turbulence kinetic energy due to the mean velocity gradients

G_b the generation of turbulence kinetic energy due to buoyancy

Y_m the contribution of the fluctuating dilation incompressible turbulence due to the overall dissipation rate

s_k the turbulent Prantel number for k

s_e the turbulent Prantel number for e

y^+ dimensionless normal distance from wall $= yu^*/v$

u^* friction velocity $= \sqrt{t_w / r}\ [m/s]$

v kinematic viscosity of water $[m^2/s]$

t_w wall shear stress $[Pa.]$

C_d discharge coefficient

C_v flow coefficient

s cavittation coefficient

SG specific gravity

References

[1] American Water Works Association (AWWA),Butterfly valves: Torque, head loss and cavitation analysis, Technical Report M49, American Water Works Association, 2001.

[2] Ellis, J. ; Mualla, W., "Dynamic behavior of safety butterfly valves", Water Power and Dam Construction, (121), 1984, 26-31.

[3] Solliec, C.; Danson, F., "Aerodynamic torque acting on a butterfly valve. Comparison and choice of a torque coefficient", Journal of Fluids Engineering, (121), 1999, 914-917.

[4] Chaiworapuek, W., "The Engineering Investigation of the Water Flow past the Butterfly Valve", Erasmus Mundus Master of Mechanical Engineering, 2007.

[5] Haynes, J., "CFD analysis of the flow past a butterfly valve", Honours thesis, University of Tasmania, 2007.

[6] ANSYS Europe Ltd, ANSYS CFX solver modeling guide, V11, Technical report, ANSYS Europe Ltd, 2007.

[7] Schlichting, H., "Boundary-Layer Theory", McGraw-Hill, 1968, 6th edition.

[8] Yeop Park, Ju.; Kyoon Chung, M., "Study on Hydrodynamic Torque of a Butterfly Valve", ASME J. Fluids Eng., 2006.